Rectification in synthetic conical nanopores: A one-dimensional Poisson-Nernst-Planck model

I. D. Kosińska
Institut für Physik, Universität Augsburg, D-86135 Augsburg, Germany
and M. Smoluchowski Institute of Physics, Jagiellonian University, PL-30-059 Kraków, Poland

I. Goychuk, M. Kostur, and G. Schmid
Institut für Physik, Universität Augsburg, D-86135 Augsburg, Germany

P. Hänggi
Institut für Physik, Universität Augsburg, D-86135 Augsburg, Germany
and Department of Physics, National University of Singapore, Singapore 117542, Republic of Singapore
(Received 11 December 2007; published 26 March 2008)

Ion transport in biological and synthetic nanochannels is characterized by phenomena such as ion current fluctuations and rectification. Recently, it has been demonstrated that nanofabricated synthetic pores can mimic transport properties of biological ion channels [P. Yu. Apel *et al.*, Nucl. Instrum Methods Phys. Res. B **184**, 337 (2001); Z. Siwy *et al.*, Europhys. Lett. **60**, 349 (2002)]. Here, the ion current rectification is studied within a reduced one-dimensional (1D) Poisson-Nernst-Planck (PNP) model of synthetic nanopores. A conical channel of a few nm to a few hundred nm in diameter, and of a few μm long is considered in the limit where the channel length considerably exceeds the Debye screening length. The rigid channel wall is assumed to be weakly charged. A one-dimensional reduction of the three-dimensional problem in terms of corresponding entropic effects is put forward. The ion transport is described by the nonequilibrium steady-state solution of the 1D Poisson-Nernst-Planck system within a singular perturbation treatment. An analytic formula for the approximate rectification current in the lowest order perturbation theory is derived. A detailed comparison between numerical results and the singular perturbation theory is presented. The crucial importance of the asymmetry in the potential jumps at the pore ends on the rectification effect is demonstrated. This so constructed 1D theory is shown to describe well the experimental data in the regime of small-to-moderate electric currents.

DOI: 10.1103/PhysRevE.77.031131 PACS number(s): 05.60.Cd, 81.07.De, 05.40.Jc

I. INTRODUCTION

The interaction of a cell with the extracellular environment through the membrane is of prominent importance for the cell behavior and cellular function. The lipid bilayer of cell membranes constitutes a barrier to the passage of charged and polar molecules [1]. The channel proteins, which form narrow hydrophilic pores, primarily allow for the passage of small inorganic ions. The opening and closing of ion channels characteristically depend on the membrane voltage or the binding of selective ligand molecules [2].

The production techniques and the application of single nanochannels in polymer films with lengths of micrometers and diameter sizes on the nanoscale is presently attracting widespread interest [3]. Synthetic nanochannels have been fabricated as mimics of real biological nanopores and ion channels [4]. A recent intriguing finding was that conically shaped nanopores can be put to work as promising sensing elements for small molecules [5], DNAs [6], proteins [7], and yet other substances [8].

The sensing and transport properties of conical nanopores are strongly dependent on the shape of the pores, i.e., on parameters such as the cone angle and its length. An important feature of charged conical nanopores in comparison to the cylindrical ones is that the voltage drop caused by the ion current is centered around the narrow tip [9].

The flow of ions through a nanopore can either be driven by concentration gradients or an electric field, or both. It can approximately be modeled by means of an electrodiffusion equation. Within this description, the electric field inside the pore is governed in a self-consistent manner by the ion concentrations via the Poisson equation. At the boundaries, both the ion (bulk) concentrations and the electrical potentials are externally fixed. This may generate a steady current flow. With this work, our objective is the derivation of the general solution of such a nonequilibrium steady-state problem. A challenge is then the investigation of the influence of an externally applied voltage on different polarity for rectification, being induced by the asymmetry of the nanopore.

A three-dimensional PNP modeling of the ion conductance in biological gramicidin A channels has been put forward in Ref. [10] for several membrane electrostatics. This three-dimensional (3D) modeling was next investigated in Ref. [11] in the context of the so-called potential-of-mean-force-Poisson-Nernst-Planck theory, which accounts for the dynamical relaxation of the channel forming protein and the surrounding medium by incorporating the free energy of inserting a single ion into the channel. Furthermore, outer membrane protein F (OmpF) and α-hemolysin porin channels were studied within similar approaches, complemented by molecular dynamics, and Brownian dynamics simulations in Refs. [12,13] and standard methods of continuum electrostatics recalled in Ref. [14]. In particular, for these porin channels, an asymmetric current-voltage characteristic, which implies a current rectification under alternating voltage conditions, has been observed. However, the structural

complexity of biological ion channels and, in particular, an inhomogeneous charge distribution on the channel wall prevented any possibility for a rigorous analytical treatment in these numerical studies. What is more, it remains unclear until now how a very popular one-dimensional, textbook [15] description of the ionic conductance of such and similar biological channels can be justified from a 3D picture if the channel's length L and diameter do not differ much, like $L/D \sim 3$ for porins.

Synthetic nanochannels [3], which have microns in length, are very much different in this respect providing a nice test bed for a one-dimensional reduced description. Such channels are wide enough (up to several nanometers in the narrowest part), so that the self-consistent mean field PNP theory, which neglects totally the correlation effects (existing e.g., due to a finite size of ions), seems well applicable. Moreover, the conductance of an ion channel in the limit, where its length exceeds largely the screening Debye length, should be strictly Ohmic [16], if the diameter does not vary and the channel wall is not charged. If the mobilities of free cations and anions are equal, the rectification effect can therefore only emerge due to a synergy of the entropic driving force caused by the channel asymmetry (conical pore) and the electrostatic effects caused by the fixed charges present on the channel wall. An analytical theory for such a system is currently absent.

With this work we shall address this challenge within a singular perturbation theory approach for long conical pores, where the pore length substantially exceeds both its diameter and the Debye length. The obtained analytical results are validated by precise numerics. Moreover, numerical results are obtained for realistic surface charge densities beyond the validity range of perturbation theory. Then, the satisfying agreement with experimental data is demonstrated.

II. IONIC TRANSPORT

Three-dimensional Poisson-Nernst-Planck (PNP) equations

We are interested in the ionic currents through relatively narrow pores which are created in a thin (of μm) dielectric film. The channel wall is assumed to be weakly charged by a prescribed surface charge density σ (see Fig. 1). The whole system is immersed in an electrolyte solution. We consider the limit of long channels with the length being much larger than both, the pore diameter and the Debye screening length: $\xi_D = \sqrt{\epsilon_0 \epsilon_w k_B T/(2e^2 N_A 10^3 I_c)}$ (in meters). Therein, ϵ_0 denotes the dielectric constant of vacuum, $\epsilon_w \approx 80$ the relative dielectric constant of water, k_B the Boltzmann constant, T the temperature, e the elementary charge, and N_A is the Avogadro number. $I_c = \Sigma_{i=\pm} \nu_i^2 c_i(\infty)/2$ defines the ionic strength of the electrolyte [15]. It is given in terms of the bulk concentration of anions $c_-(\infty)$, and cations $c_+(\infty)$ (in molars $\equiv$ mol/liter, M), respectively, with the valences being ν_i. For monovalent electrolytes, i.e., $\nu_i = \pm 1$, with $c_+(\infty) = c_-(\infty) = 1M$, the ionic strength is $I_c = 1M$ and thus $\xi_D \approx 0.305$ nm at room temperature $T = 298$ K. This presents a typical experimental situation for the synthetic pores studied in Refs. [3,4,7], where $\xi_D \sim 1$ nm at submolar concentrations of approximately $0.1M$. Our electrolyte system consists of two kinds of ions: potassium, K^+, and chloride, Cl^-.

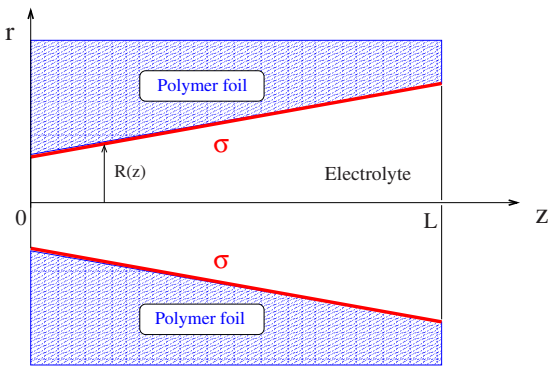

FIG. 1. (Color online) A sketch of the profile of the conical nanopore. The wall inside the pore exhibits a surface charge density σ. The local radius of the pore $R(z)$ is given by Eq. (5). The drawing does not reflect the actual physical $(z:r)$ proportions.

Let us next start from the 3D electrodiffusion equation

$$\frac{\partial c_i(\vec{r},t)}{\partial t} = -\vec{\nabla} \cdot \vec{j}_i(\vec{r},t), \tag{1}$$

where

$$\vec{j}_i(\vec{r},t) = -D_i \vec{\nabla} c_i(\vec{r},t) + e\nu_i \mu_i \vec{\mathcal{E}}(\vec{r}) c_i(\vec{r},t) \tag{2}$$

defines the mass *flux density* $\vec{j}_i$ of the ith species of ions, $\vec{r}$ is the position vector, D_i is the diffusion constant, μ_i is the mobility of the ion particles, and $\vec{\mathcal{E}}$ denotes the electric field. The consistency with the thermal equilibrium demands that the mobility of the ions μ_i fulfill the Sutherland-Einstein relation, reading $D_i = \mu_i/\beta$, with the inverse temperature $\beta = 1/k_B T$. Because $\vec{\mathcal{E}}(\vec{r}) = -\vec{\nabla}\Phi(\vec{r})$, where $\Phi(\vec{r})$ is the electric potential, one can recast Eq. (1) into the more convenient form,

$$\frac{\partial c_i(\vec{r},t)}{\partial t} = D_i \vec{\nabla} \cdot \left(\exp[-e\nu_i \beta \Phi(\vec{r})] \vec{\nabla} \exp[e\nu_i \beta \Phi(\vec{r})] c_i(\vec{r},t) \right). \tag{3}$$

The appropriate choice of coordinates for the problem at hand are the cylindrical coordinates (r, ϕ, z). The electric potential $\Phi(r,z)$ is governed in a self-consistent manner by the Poisson equation

$$\epsilon_0 \vec{\nabla} \cdot [\epsilon(r,z) \vec{\nabla} \Phi(r,z)] = -\sum_i \rho_i(r,z) - \rho_{\text{fix}}(r,z). \tag{4}$$

The ion concentration c_i (in molars) is related to the density of electric charge ρ_i (in units of Coulombs per cubic meter, C/m^3) through $\rho_i = 10^3 e\nu_i N_A \Theta[-r + R(z)] c_i$, where Θ is the Heaviside step function, and

$$R(z) = R(0) + [R(L) - R(0)]z/L \tag{5}$$

denotes a variable cone radius. The nanochannel radii at the left and right pore ends are $R(0)$ and $R(L)$, respectively, and L is the length of the pore. The charge density ρ_{fix}

$=\delta[r-R(z)]\sigma$, with $\delta(x)$ being the Dirac delta function, represents the fixed charges located on the inside of the channel wall. $\epsilon(r,z)=\epsilon_p\Theta[r-R(z)]+\epsilon_w\Theta[-r+R(z)]$ describes dielectric properties of the open nanopore, where ϵ_p, ϵ_w are the relative dielectric constants of the polymer and water, respectively. The set of relations (3) and (4) for $\vec{\nabla}\cdot\vec{j}_i=0$ constitutes the system of coupled Poisson-Nernst-Planck (PNP) equations.

III. ONE-DIMENSIONAL MODEL REDUCTION FOR LONG PORES

The primary purpose of our work is to gain analytical insight into the nature of rectification current. Since an analytical solution for the 3D PNP in general could not be found, a simplification is unavoidable. The ion diffusion and the ion flow are confined by the channel to a variable cross-section area $\pi R^2(z)$. Assuming local equilibrium in the transverse (r) direction, the full three-dimensional system can be cast into an effective one-dimensional problem. The price to be paid is the emergence of an additional, entropic potential contribution $\Delta S(z)$ [17–20]. Moreover, as pointed out by Zwanzig [17], a renormalization of the diffusion coefficient emerges as a dynamical effect due to a finite relaxation time in the transversal direction. In our situation (i.e., for a small opening angle of the cone) this latter dynamical correction to the diffusion coefficient is negligible [21]. If the resulting currents are too large these model assumptions cannot be justified, as the particles must have sufficient time to relax into the transverse direction [20].

In cylindrical coordinates (r,ϕ,z) the equation for mass current due to the coaxial symmetry assumes the form

$$\begin{aligned}\vec{j}_i(r,z,t) = &- D_i \exp[-e\nu_i\beta\Phi(r,z)]\frac{\partial}{\partial r}\\ &\times\exp[e\nu_i\beta\Phi(r,z)]c_i(r,z,t)\hat{r} - D_i\\ &\times\exp[-e\nu_i\beta\Phi(r,z)]\frac{\partial}{\partial z}\\ &\times\exp[e\nu_i\beta\Phi(r,z)]c_i(r,z,t)\hat{z},\end{aligned} \tag{6}$$

where $\hat{r}$ and $\hat{z}$ are the units vectors in cylindrical coordinates.

The steady-state regime is described by the condition

$$\vec{\nabla}\cdot\vec{j}_i = 0. \tag{7}$$

Because the length of the channel by far exceeds its diameter, we can assume local equilibrium, i.e., uniform distributions for the ions and a constant potential across each channel cross section,

$$c(z,r,t)\approx c(z,t), \quad \Phi(r,z,t)\approx\Phi(z,t). \tag{8}$$

The validity of an instant local equilibrium in transversal direction is fulfilled for weakly charged channel walls and not too large ion flow through the channel. Under this assumption, it is possible to reduce the complex original 3D problem to a simpler, effective one-dimensional description.

Using the divergence of a given vector $\vec{u}$,

$$\vec{\nabla}\cdot\vec{u} = \lim_{\Delta z\to 0}\frac{1}{A(z)\Delta z}\oint_S \vec{u}\cdot\hat{n}dS, \tag{9}$$

where $V(z)=A(z)\Delta z$ denotes the volume surrounded by the closed surface S with the normal vector $\hat{n}$, and the fact that no ion flux across the channel wall occurs, Eq. (1) can be reduced [22] under the assumptions in Eq. (8) to the form

$$\frac{\partial\bar{c}_i(z,t)}{\partial t} = \frac{\partial}{\partial z}\left\{\nu_i e\beta D_i\bar{c}_i(z,t)\frac{\partial\Phi(z)}{\partial z} + A(z)D_i\frac{\partial}{\partial z}\frac{\bar{c}_i(z,t)}{A(z)}\right\}, \tag{10}$$

wherein $\bar{c}_i(z,t)=10^3c_i(z,t)A(z)$ denotes the one-dimensional concentrations (in mol per meter).

Likewise, using Eq. (9) and the electrostatic boundary condition on the channel wall, reading

$$\epsilon_p\mathcal{E}^{\perp}_{\text{polymer}} - \epsilon_w\mathcal{E}^{\perp} = \sigma, \tag{11}$$

the 3D Poisson equation is effectively reduced [22,23] into the form

$$\begin{aligned}\epsilon_0\epsilon_w\frac{d^2\Phi(z)}{dz^2} = &-\frac{2\sigma}{R(z)} - eN_A\sum_i \nu_i\frac{\bar{c}_i(z,t)}{A(z)}\\ &-\epsilon_0\epsilon_w\frac{d\Phi(z)}{dz}\frac{d}{dz}\ln A(z).\end{aligned} \tag{12}$$

The quantity $2\sigma/R(z)$ has the meaning of the volume density of the fixed surface charge $\rho=\Delta Q/\Delta V$, where $\Delta Q=2\pi\sigma R(z)\Delta z$ and $\Delta V=\pi R^2(z)\Delta z$.

Likewise, Eq. (10) can be recast as

$$\begin{aligned}\frac{\partial\bar{c}_i(z,t)}{\partial t} &= -\frac{\partial}{\partial z}J_i(z,t)\\ &= \frac{\partial}{\partial z}\left\{D_i\exp[-\beta G_i(z)]\frac{\partial}{\partial z}\bar{c}_i(z,t)\right.\\ &\quad\left.\times\exp[\beta G_i(z)]\right\},\end{aligned} \tag{13}$$

where J_i denotes mass fluxes, and $G_i(z)$ is the free energy (potential of mean force), given by

$$G_i(z) = -TS(z) + e\nu_i\Phi(z). \tag{14}$$

Due to the reduction from 3D into 1D it inherits the entropic contribution

$$S(z) = k_B\ln[A(z)/A_0], \tag{15}$$

where A_0 denotes an arbitrary, but irrelevant reference cross-section area. The coupled nonlinear equations (12) together with the set of Eqs. (13)–(15) present a self-consistent, reduced 1D electrodiffusion equation, which is similar in spirit to the well-known reduction of a 3D-diffusion problem to an effective Fick-Jacobs diffusion equation [17–20]. The dependence $R(z)$ is still arbitrary within the discussed approximations; its variation must be smooth, however, such that the z variations of the normal to the channel's surface from the cylindrical geometry become negligible up to the second or-

der. This constructed 1D Poisson-Nernst-Planck modeling generalizes the one given in Ref. [22] for strictly cylindrical pores to nanopores possessing a variable cross-section diameter.

A. Evaluation of the electric currents

We consider the steady-state, nonequilibrium solutions characterized by constant mass fluxes J_i. The corresponding electric currents are $I_i = F\nu_i J_i$, where F denotes the Faraday constant. Explicitly, these electric currents for the ith ion species read

$$I_i = -FD_i\nu_i \exp[-\beta G_i(z)]\frac{d}{dz}\exp[\beta G_i(z)]\bar{c}_i(z). \quad (16)$$

Thus, currents are fully determined by the bulk ion concentrations and the electric potential difference $U=\Phi(0)-\Phi(L)$ across the membrane, as determined by the effective 1D Poisson-Nernst-Planck equations.

B. Dimensionless equations

For the sake of convenience we perform all our numerical and analytical calculations in dimensionless variables. In doing so, we transform the Poisson-Nernst-Planck equations to their dimensionless form by the use of the following relations: $z^\star = z/L$, $R^\star(z)=R(z)/R(0)$, $\Phi^\star(z)=\beta e\Phi(z)$, $I_i^\star = I_i L/(FD_i c_0)$, and $\bar{c}_i^\star(z)=c_i(z)/c_0$, where c_0 is a reference 1D concentration (in $1/6.023\times 10^{-14}$ mole/m). Then, the equation for the constant electric currents assume the appealing form

$$\nu_i I_i^\star + \frac{d}{dz^\star}\bar{c}_i^\star + \nu_i\bar{c}_i^\star\frac{d\Phi^\star}{dz^\star} - \bar{c}_i^\star\frac{2}{R^\star}\frac{dR^\star}{dz^\star} = 0, \quad (17)$$

and Eq. (12) transforms into

$$\frac{1}{\lambda^2}\left(\frac{d^2\Phi^\star}{dz^{\star 2}} + \frac{2}{R^\star}\frac{dR^\star}{dz^\star}\frac{d\Phi^\star}{dz^\star}\right) + \frac{\epsilon}{R^\star} + \frac{1}{\pi R^{\star 2}}\sum_i \nu_i\bar{c}_i^\star = 0, \quad (18)$$

with

$$\frac{1}{\lambda^2} = \frac{\epsilon_0\epsilon_w R^2(0)}{c_0 F\beta e L^2}, \quad (19)$$

and the effective dimensionless surface charge density

$$\epsilon = \frac{2\sigma R(0)}{c_0 F}. \quad (20)$$

Below, upon simplifying the notations, we shall suppress the notation with the superscript (*).

C. Boundary conditions

We next solve the system of equations (17) and (18) with the following boundary conditions:

$$\bar{c}_{K^+}(0) = \pi c_{K^+,L}, \quad \bar{c}_{Cl^-}(0) = \pi c_{Cl^-,L},$$

$$\bar{c}_{K^+}(1) = \pi(1+\gamma)^2 c_{K^+,R}, \quad \bar{c}_{Cl^-}(1) = \pi(1+\gamma)^2 c_{Cl^-,R},$$

$$\Phi(0) = 0, \quad \Phi(1) = \Phi_R, \quad (21)$$

wherein $\gamma=[R(L)-R(z=0)]/R(z=0)$, $c_{i,\{L,R\}}=10^3 c_{\mathrm{bulk},\{L,R\}}\times R^2(z=0)/c_0$, and $c_{\mathrm{bulk},\{L,R\}}$ denote the bulk concentrations of ions on the left and right sides, respectively. The electroneutrality condition yields $c_{K^+,L}=c_{Cl^-,L}=c_L$ and $c_{K^+,R}=c_{Cl^-,R}=c_R$. Furthermore, the difference of dimensionless potentials across the nanopore is related to the applied voltage U (in units of volts) by $\Phi(0)-\Phi(1)=\beta eU$, yielding $U=-\Phi(1)/(\beta e)$.

IV. SINGULAR PERTURBATION THEORY

The corresponding 1D system contains two small parameters, namely,

(i) $1/\lambda$, in Eq. (19), which is proportional to the ratio of the Debye length ξ_D to the channel length L;

(ii) the scaled surface charge density ϵ [see Eq. (20) and the Appendix].

In our case, i.e., a long nanopore with a typical length $L=12\,000$ nm, $1/\lambda$ is of the order of 10^{-5} for submolar concentrations. The parameter ϵ is of the order of 10^{-1}, or larger. Therefore we will focus on the leading term in the limit $1/\lambda\to 0$, while ϵ will be considered as a regular series expansion parameter. Thus, the problem requires one to use a singular perturbation theory in $1/\lambda$ and a regular expansion in ϵ. We use the standard method of matched asymptotic expansions [24] and seek for an approximate solution of Eqs. (17) and (18) in the form

$$\Phi = \Phi^{(0)} + \frac{1}{\lambda}\Phi^{(1)} + \cdots,$$

$$\bar{c}_{K^+} = c_{K^+}^{(0)} + \frac{1}{\lambda}c_{K^+}^{(1)} + \cdots,$$

$$\bar{c}_{Cl^-} = c_{Cl^-}^{(0)} + \frac{1}{\lambda}c_{Cl^-}^{(1)} + \cdots. \quad (22)$$

Since the small parameter $1/\lambda^2$ appears in Eq. (18) in front of the derivatives, we are dealing with a typical singularly perturbed boundary-value problem.

Below we consider a symmetric bulk situation with equal ion concentrations on both membrane sides, $c_L=c_R=c$. After cumbersome calculations the uniformly valid approximation on [0,1] is found in the first order of ϵ to read

$$\Phi(z) \approx \Phi^{(0)}(z) = \Phi_0(z) - \epsilon\left\{\phi_1^L(\lambda z) + \Phi_1(z) + \phi_1^R[\lambda(1-z)] + \frac{1}{2c} + \frac{1}{2c(1+\gamma)}\right\} + O(\epsilon^2), \quad (23)$$

$$\bar{c}_{\{K^+,Cl^-\}}(z) = \frac{1}{2}c_{\Sigma,0}(z) - \frac{1}{2}\epsilon\{\pm\pi/R(z) + c_{\Sigma,1}(z) \mp 2\pi c\phi_1^L(\lambda z) \mp 2\pi c(1+\gamma)^2 \times\phi_1^R[\lambda(1-z)] \mp \pi(2+\gamma)\} + O(\epsilon^2), \quad (24)$$

where the upper sign refers to K^+ ions, and the lower one to Cl^-, respectively, and the expressions

$$c_{\Sigma,0}(z) = \left(\frac{-J_0}{\gamma R(z)} + C_0\right) R^2(z) = C_0 R^2(z),$$

$$\Phi_0(z) = \frac{I_0}{\gamma C_0}\frac{1}{R(z)} + E_0 = \Phi_R \frac{(1+\gamma)z}{R(z)},$$

$$c_{\Sigma,1}(z) = \left(-\frac{\pi I_0}{2\gamma C_0}\frac{1}{R^2(z)} - \frac{J_1}{\gamma R(z)} + C_1\right) R^2(z)$$

$$= \frac{1}{2}\pi\Phi_R\gamma(z-1)z,$$

$$\Phi_1(z) = \frac{I_0}{C_0^2\gamma}\left(\frac{\pi I_0}{6\gamma C_0}\frac{1}{R^3(z)} + \frac{J_1}{2\gamma}\frac{1}{R^2(z)} - \frac{C_1}{R(z)}\right) + \frac{I_1 - \pi\gamma}{C_0\gamma R(z)} + E_1, \tag{25}$$

contain eight constants $C_0, C_1, I_0, I_1, J_0, J_1, E_0, E_1$ which are determined from the matching conditions (see the Appendix). Furthermore, the left or right boundary layer potential variations in Eqs. (23) and (24) are given, respectively, by

$$\phi_1^L(\lambda z) = \frac{1}{2c}(\exp[-\sqrt{2c}\lambda z] - 1),$$

$$\phi_1^R[\lambda(1-z)] = \frac{1}{2c(1+\gamma)}(\exp[-\sqrt{2c}\lambda(1-z)] - 1), \tag{26}$$

where $\sqrt{2c}\lambda/L = 1/\xi_D$, with ξ_D being the Debye length in bulk.

Assuming that both sorts of ions have equal diffusion coefficients [26], i.e., $D_{K^+} = D_{Cl^-} = D$, the two constants $J = -I_{K^+} + I_{Cl^-}$ and $I = I_{K^+} + I_{Cl^-}$ (see Ref. [25]) have the following physical meaning: $J = J_0 - \epsilon J_1 + O(\epsilon^2)$ yields an approximation to the negative of the total mass current, whereas $I = I_0 - \epsilon I_1 + O(\epsilon^2)$ approximates the total electric current,

$$I \approx -2\pi c(1+\gamma)\Phi_R\left(1 + \epsilon\frac{1}{24c}\frac{\gamma}{1+\gamma}\Phi_R\right). \tag{27}$$

Equation (27) presents a main analytical result of this paper. In the original physical variables it reads

$$I = I_{K^+} + I_{Cl^-} \approx 2\pi F D c_{bulk}[R(0)R(L)/L](eU/k_BT) \times\left[1 - \frac{1}{12}\frac{\sigma}{c_{bulk}F}\left(\frac{1}{R(0)} - \frac{1}{R(L)}\right)\frac{eU}{k_BT}\right], \tag{28}$$

where c_{bulk} is the concentration of ions in bulk.

It shows that the rectification effect appears already in the first order of ϵ. The effect vanishes, when the pore is not charged, $\sigma = 0$. This is because the rectification effects for the monovalent cations and anions for an uncharged pore are (trivially) "counterdirected" and compensate each other exactly if both sorts of ions have equal diffusion coefficients. Obviously, for the cylindrical pore with $\gamma = 0$, it goes away as well. Apparently, the current rectification is thus due to a synergy of the entropic effect caused by the pore asymmetry and the present surface charge. Moreover, one can attribute this result also to different volume charge densities $2\sigma/R(z)$ of the fixed charges at both channels ends. Given this latter interpretation, one can expect also rectification effect for inhomogeneously charged cylindrical pores with two very different charge densities at the ends.

Using the computer algebra system MAPLE, we obtained also analytical results for electric currents and fluxes (*total* and individual) up to fourth order in ϵ. The results are, however, rather cumbersome and of limited analytical insight, and thus are not explicitly displayed here. We evaluated them though numerically (see the corresponding figures given below). Furthermore, the PNP system in Eqs. (17) and (18) with the boundary conditions in Eq. (21) was integrated numerically by making use of a collocating method with adaptive meshing [27]. The results of the analytical perturbation theory and the numerical solutions compare very favorably where the perturbation theory is expected to work properly.

V. RESULTS AND NUMERICAL COMPARISON

A. Perturbation theory vs numerics

We consider channels with some fixed left opening radius $R(z=0) = 3$ nm and two different right opening radii:

(1) "long pore": $L = 12\,000$ nm, $R(L) = 220$ nm

(2) "short pore": $L = 200$ nm, $R(L) = 6.616$ nm.

In both cases the opening angle of the cone is identical, $\psi = 2\arctan\{[R(L) - R(z=0)]/L\} \approx 2°$. Furthermore, two different surface charge densities are used in our studies, namely, $\sigma = -0.02, -0.1$ e/nm^2. The first one corresponds to a parameter value $\epsilon = 0.12$, which is well within the regime of validity of the perturbation scheme. For the second value we have $\epsilon = 0.6$ for which we already expect the perturbation method to fail, but it still might work occasionally. Furthermore, the diffusion coefficients were taken as $D_{K^+} = D_{Cl^-} = 2 \times 10^9$ nm^2/s, see in [26], temperature $T = 298$ K and $\epsilon_w = 80$. The concentration profiles for both, the singular perturbation solution and the numerical solution are depicted in Fig. 2. The first order approximation agrees very well with numerical solution for the small surface charge density of $\sigma = -0.02$ e/nm^2. However, this agreement is worsening upon increasing the values of σ. For the moderately large charge density $\sigma = -0.1$ e/nm^2 the discrepancy between the exact solution and analytical approximation becomes already significant. In the inset in Fig. 2 we show the left and the right boundary layers, according to Eq. (24). Both layers possess a width of several Debye lengths ξ_D. In the case of the "long pore", the increase of the concentration $c_{K^+}(z)$ within the boundary layer is more distinct near the narrow opening (the boundary $z = 0$), as compared to the wide opening at the right boundary at $z = L$ [see Fig. 2(b)]. This is so because for this channel the right opening radius $R(L) = 220$ nm is very wide. The shorter channel with left and right opening radii of similar size does not display such a striking difference.

B. Current-voltage characteristics and rectification

In Figs. 3 and 4 we depict the current-voltage $(I-U)$ characteristics of the ion transport. The comparison of analytical

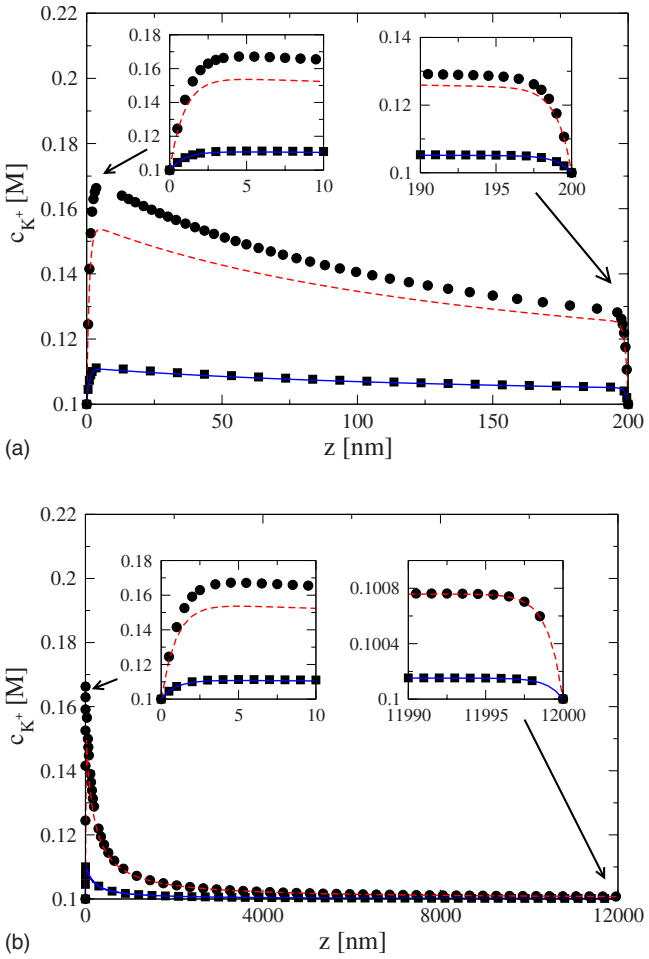

FIG. 2. (Color online) Concentration profile $c_{K^+}(z)$ at equilibrium ($c_L=c_R=0.1M$, $\Phi(z=0)=\Phi(z=L)=0$). Calculations are done for the short pore (a) and the long pore (b). Solid line and squares: $\sigma=-0.02$ e/nm^2; dashed line and circles: $\sigma=-0.1$ e/nm^2. Symbols in all cases denote the results of the numerical solution, and lines represent the results of the perturbation theory. The insets depict a closer look into the left and the right boundary layers, respectively.

and numerical results show that the currents for both the short pore [Fig. 3(a)] and the long pore [Fig. 3(b)] are well predicted by the first order perturbation theory, cf. Eq. (28), in the range of U from −0.1 V to 0.1 V, for both surface charge densities $\sigma=-0.02$ e/nm^2 and $\sigma=-0.1$ e/nm^2. However, for the larger density, the agreement deteriorates for the short pore. As expected, the discrepancy grows further with increasing the absolute value of the applied voltage U across the nanopore (cf. Fig. 4).

The above examples evidence that the first order perturbation expansion works well only for a relatively small charge density σ and not too large applied voltages. However, in a wider range of voltages and for larger charge densities one has to use a higher order perturbation theory in ϵ.

In Fig. 5, we depict the numerical $I-U$ current-voltage characteristics for both the potassium I_{K^+}, and the chloride I_{Cl^-} currents versus the fourth order perturbation theory results. The found agreement is rather good. Undoubtedly, the characteristics are strongly nonlinear and asymmetric. Consequently, the nanopore exhibits rectification properties. We can analytically describe this effect in the first order of ϵ. Then, the individual ionic currents are approximated by the following expansions: $I_{K^+}=(I_0-J_0)/2-\epsilon(I_1-J_1)/2+O(\epsilon^2)$ and $I_{Cl^-}=(I_0+J_0)/2-\epsilon(I_1+J_1)/2+O(\epsilon^2)$. Interestingly, for both the potassium and the chloride currents the difference between the absolute values of positive and negative current branches is the same and is equal to

$$|I_{\{K^+,Cl^-\}}(U)|-|I_{\{K^+,Cl^-\}}(-U)| \approx -\epsilon I_1 = -\frac{1}{6}D\pi\sigma\frac{R(L)-R(0)}{L}\left(\frac{eU}{k_BT}\right)^2. \quad (29)$$

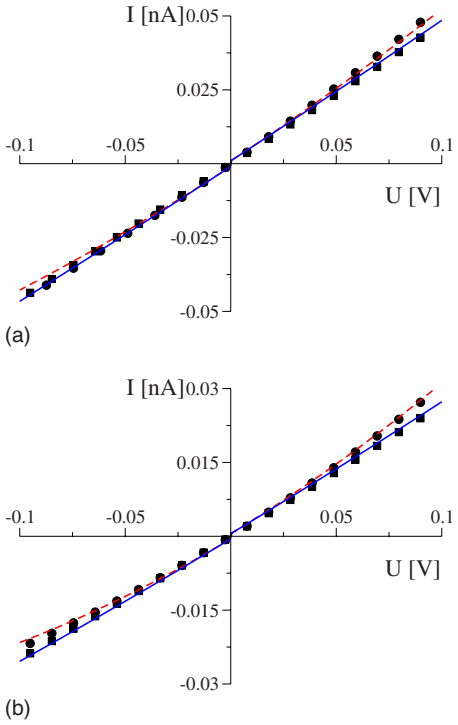

FIG. 3. (Color online) Current voltage ($I-U$) characteristics of the short pore (a) and the long pore (b) for U from −0.1 V to 0.1 V. Solid line and squares: $\sigma=-0.02$ e/nm^2; dashed line and circles: $\sigma=-0.1$ e/nm^2. Symbols denote the numerical solution, and the lines represent the results of first order perturbation theory (in ϵ).

In a negatively charged nanopore, cations experience a potential well, whereas anions sense a potential barrier. Thus, the potassium concentration and also the potassium current are always larger than those of chloride (see Fig. 5). This effect becomes enhanced upon increasing the absolute value of the (negative) charge density σ. However, the equivalent asymmetry of the $I-U$ dependence for individual currents indicates that the rectification quality of the pore is independent of the ion sign within this order of perturbation theory.

Furthermore, in Fig. 6(a) we compare the electric potential profiles $\Phi(z)$ of the short pore ($L=200$ nm, squares) and the long pore ($L=12\,000$ nm, circles) for the equilibrium situation. They coincide up to $z=195$ nm, because the angle of the cones of both nanopores are the same. This implies

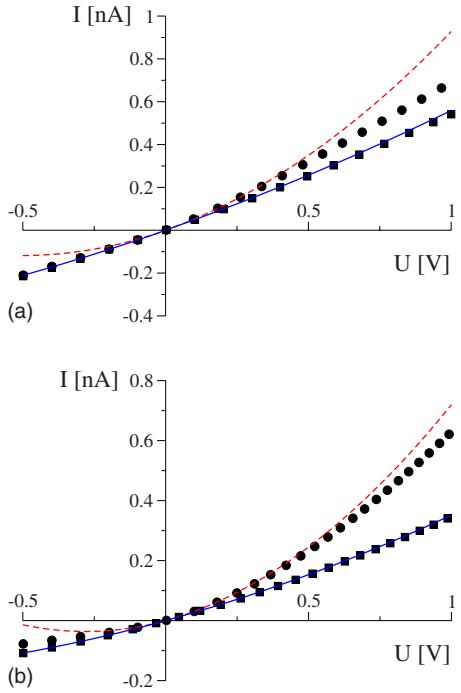

FIG. 4. (Color online) Current voltage ($I-U$) characteristics of the short pore (a) and the long pore (b) for U from −0.5 V to 1 V. Solid line and squares: $\sigma=-0.02$ e/nm^2; dashed line and circles: $\sigma=-0.1$ e/nm^2. Symbols in all cases stand for numerical solution, and lines represent first order perturbation theory (in ϵ).

that the electric field profiles in the narrow parts of both channels are identical. Since the rectification efficiency seemingly is caused mostly by the sharp potential variations in the narrow regions, one might naively expect that the rectification quality will be similar for both cases, even if the absolute $I-U$ characteristics for these two nanopores are rather different [cf. Fig. 6(b)]. However, this would be an incorrect conclusion.

Indeed, the absolute values of the *total* electric current $I=I_{K^+}+I_{Cl^-}$ is lower for the long pore as compared to the short pore. This result corroborates with the higher resistance of the longer pore. To quantify the rectification effect, we define the quantity

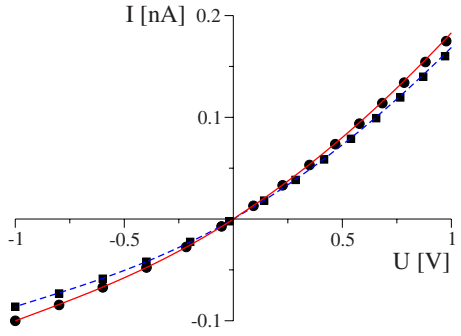

FIG. 5. (Color online) The potassium and chloride currents in the short pore for $\sigma=-0.02$ e/nm^2. The solid line represents the fourth order (in ϵ) perturbation calculation for potassium and the dashed line for the chloride current. Symbols in all cases present the numerical solution (circles: potassium current; squares: chloride).

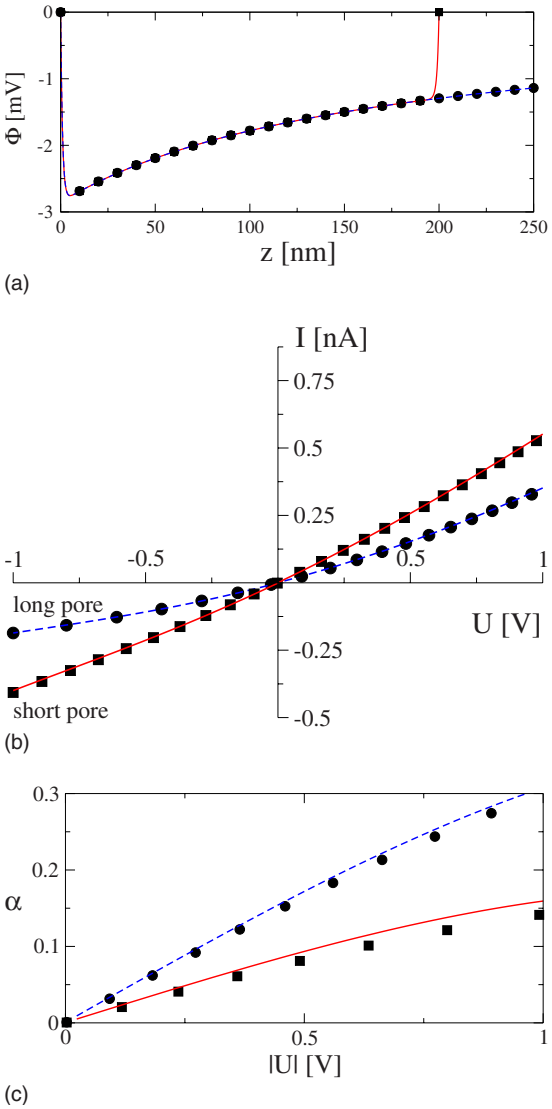

FIG. 6. (Color online) In panel (a) we depict the potential profile $\Phi(z)$ at equilibrium ($c_L=c_R=0.1M$, $\Phi(0)=\Phi(L)=0$) for $\sigma=-0.02$ e/nm^2. In panel (b) we depict the $I-U$ dependence and in panel (c) we show the rectification measure α. The calculations are done for the long pore (dashed line and circles) and the short pore (solid line and squares). The symbols in all cases stand for numerical solution; the lines represent the perturbation theory (in ϵ): up to second order (a), and in (b) and (c) up to fourth order.

$$\alpha=\frac{|I(U)|-|I(-U)|}{|I(U)|+|I(-U)|} \tag{30}$$

as a rectification measure. For it, the lowest order perturbation theory result in Eq. (28) yields

$$\alpha\approx-\frac{1}{24}\frac{1}{c_{\text{bulk}}F}\left(\frac{2\sigma}{R(0)}-\frac{2\sigma}{R(L)}\right)\frac{e|U|}{k_BT}. \tag{31}$$

As seen from this expression, the quality of rectification α, does not depend on the channel length L and is determined rather by the difference of the inverse radii and by the surface charge. Note that, in the above-described model, the

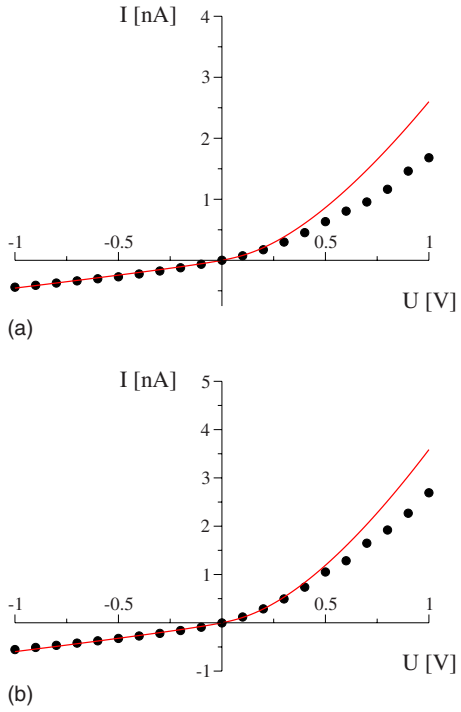

FIG. 7. (Color online) The current voltage ($I-U$) dependence in the experiment (symbols) and the 1D-PNP theory (lines). Only the numerical results are given because the perturbation approach fails for the large surface charges used in the experiment. We depict results for one value of the surface charge density $\sigma=-1.0$ e/nm^2 and for $c_L=c_R=0.1M$, which lies within the range of experimentally measured values. We use two different pore geometries: panel (a) $R(z=0)=3$ nm, $R(L)=265$ nm, $L=12\,000$ nm; panel (b) $R(z=0)=3.5$ nm, $R(L)=340$ nm, $L=12\,000$ nm.

volume charge density is given by $\sigma(z)=2\sigma/R(z)$ [Eq. (12)], where $R(z)$ denotes a variable cone radius. The geometry of the charged conical pore results not only in the presence of entropic potential in the 1D current equation [Eq. (16)] but also in the asymmetrical volume charge distribution $\sigma(z)$ in the reduced 1D Poisson equation [Eq. (12)]. This fact gives strong indication that in conical pores the rectification is mainly due to different potential jumps in the boundary layers at both ends of the channel. This is in line with the previous statement that the $I-U$ characteristics of the nanopore depend crucially on the total asymmetry of the potential profile [28]. Accordingly, α reveals [cf. Fig. 6(c)], that the long pore acts as a better rectifier, despite its larger resistance. However, this is not due to a larger length, but due to a larger $R(L)$.

Theory vs experiment

In Fig. 7, a comparison between the experimental data [29] and theoretical results is presented for two different nanopores of length $L=12\,000$ nm with the radii $R(0)=3.5$ nm, $R(L)=340$ nm and $R(0)=3$ nm, $R(L)=265$ nm, respectively. The experimental charge density is not known precisely. The assumed value is approximately $\sigma=-1.0$ e/nm^2, which corresponds to $\epsilon\approx 6$. This parameter value is clearly beyond the validity range of perturbation theory. Nevertheless, one can use numerics. Given the approximate, reduced character of the studied 1D Poisson-Nernst-Planck model, the semiquantitative agreement between the theory and the experiment is quite satisfactory.

Indeed, the agreement is rather satisfactory for not too large currents, $I<0.5$ nA. The simplest explanation for the discrepancy occurring for strong currents could be the violation of the condition of a local equilibrium in the transverse direction (see Sec. III). Then, this breakdown of the 1D description would be similar in nature to the one observed for diffusive transport of biased, noninteracting particles [19–21]. To fully justify this statement, one can follow the analysis in Ref. [20] to find the different time scales characterizing the problem, i.e., the time scale for diffusion in the transverse direction and the time scale associated with the drift of the ith ion along the axial direction. By comparison of these two time scales one could find out whether transported ions have enough time to relax in the transversal direction. However, in the present, more complicated situation the proposed consideration results in a very rough and somewhat vague estimation (because of a heterogeneous distribution of the ions and the corresponding electrical field along the pore). For better agreement a 3D-PNP modeling would be called for.

Such a 3D-PNP study, would in a natural way, reveal the dependence of the electric potential on the radial coordinate r, and, in turn, a heterogeneous distribution of ions in the transverse direction, contrary to the model assumptions in Eq. (8). Clearly, the larger is the surface charge density, the stronger will be the violation of these model assumptions. Because of a negatively charged channel wall, the positive ions should adhere to it forming an electrical double layer of the width ξ_D with an exponentially enhanced concentration of cations. A physical criterion to disregard this complexity can be obtained by demanding that the electrostatic energy per ion near the channel wall (in the absence of external voltage), $eV\sim e\sigma\xi_D/(\epsilon_0\epsilon_w)$, is smaller than k_BT. For $\epsilon_w=80$ and $\xi_D=1$ nm this yields $|\sigma|<0.1$ e/nm^2. For higher surface charge densities (like in the experiment) not only the homogeneity assumptions become increasingly violated, but also the surface current contributions [30,31] cannot be neglected. These effects are beyond our description within a 1D-PNP reduction. Moreover, for higher concentrations $c\sim 1M$ the ion-size effects become important [15,32] implying the presence of ion correlations. This goes beyond the mean field description.

To summarize, a numerical study of the full three-dimensional setup would be helpful in order to distinguish between the principal shortcomings of the PNP approach and the failure of our 1D reduction for large currents and/or high surface charge densities. In particular, the overall failure of the PNP approach can be due to formation of the Stern layer of condensed counterions on the pore wall [15]. Such a layer will screen and renormalize (i.e., decrease) the surface charge density "seen" by other mobile ions, thus reducing the "volume" rectification effect. A proper treatment of the surface current rectification effects in such a layer would bring about the theme of strong correlations in the ionic transport which is beyond the scope of this work.

VI. SUMMARY AND CONCLUSION

In this paper we provided an analytical treatment of the problem of current rectification by artificial conical nanopores made in synthetic membranes of about submicron-to-micron width. Within a one-dimensional reduction of the original three-dimensional problem, we have derived 1D-PNP equations [cf. Eqs. (12)–(14)], which incorporate both the entropic effects and the charge density renormalization due to the variable diameter of the tube. These equations generalize the 1D-PNP equations in Ref. [22] to the case of pores of a variable diameter.

Furthermore, we provided a singular perturbation treatment of the problem of ion conductance and rectification within the reduced 1D-PNP description implementing rigorous boundary conditions (21). Our theory applies to nanopores with lengths exceeding largely the Debye length and the pore diameter. The developed theory corresponds precisely to the experiments done by Siwy *et al.* [29]. The validity range of perturbation theory requires, however, that the channel wall is charged weakly. Then, it agrees well with the numerical solution of the 1D-PNP problem for charge densities up to $|\sigma|=0.02$ e/nm^2. Unfortunately, the experimental charge densities are much larger, about $|\sigma|\sim 1$ e/nm^2. Here the perturbation theory fails. However, the 1D-PNP equations can be integrated numerically and the obtained numerical solutions provide a good agreement with the experimental data by Siwy *et al.* [29] for sufficiently small currents.

Moreover, we quantify the rectification properties of conical nanopores. In the lowest order perturbation theory we obtained analytic formulas for the rectification current I and the rectification measure α [see Eq. (30)]. The latter measure clearly indicates that the rectification property is caused by the difference in the volume charge density of the fixed charges. In other words, the rectification is due to an asymmetry in the potential jumps at the channel ends.

A discrepancy between the experiment and the 1D-PNP modeling for large positive voltages most likely indicates the violation of the condition of local equilibrium in the transverse direction at strong currents (cf. Fig. 7). For this reason, the description within the 1D-PNP modeling breaks down and a full 3D-PNP treatment becomes necessary. We conjecture that the numerical solution of the 3D-PNP equation will provide satisfactory agreement with the experimental data for the electrolytic solutions of monovalence ions.

ACKNOWLEDGMENTS

The authors express thanks to Professor Zuzanna Siwy for providing us with her experimental data and for helpful discussion. This work has been supported by Volkswagen Foundation (project No. I/80424), the Alexander von Humboldt Foundation (I.D.K.), the DFG (research center, SFB-486, project No. A10), and by the German Excellence Initiative via the *Nanosystems Initiative Munich (NIM)* (P.H.).

APPENDIX: STUDY CASE OF SINGULAR PERTURBATION THEORY

We consider a set of two coupled differential equations (17) and (18) with the boundary conditions given in Eq. (21). Each of these equations one can be presented in the form

$$P_{1/\lambda,\epsilon}(y)=0, \tag{A1}$$

where $y=\{\bar{c}_{K^+},\bar{c}_{Cl^-},\Phi\}$ and where two small parameters $1/\lambda$ and ϵ determine the behavior of the solution. The solution shall be denoted by $y_\epsilon^{(1/\lambda)}$. The limiting problem $(1/\lambda=0)$

$$P_{0,\epsilon}(y)=0 \tag{A2}$$

possesses the solution $y_\epsilon^{(0)}$. The character of the problem changes discontinuously at $1/\lambda=0$. This implies that we have a singular perturbation in this very parameter.

1. Outer approximation

In the outer region (corresponding to the interior of the 1D channel) we approximate $y_{\text{outer}}^{(0)}(z)=\{\bar{c}_{K^+}^{(0)}(z),\bar{c}_{Cl^-}^{(0)}(z),\Phi^{(0)}(z)\}$ by use of the regular perturbation expansion as follows:

$$y_{\text{outer}}^{(0)}(\epsilon,z)=y_0(z)+\epsilon y_1(z)+\epsilon^2 y_2(z)+\cdots. \tag{A3}$$

2. Boundary layers

The region near the boundaries at $z=0$ and $z=1$ wherein y is changing rapidly presents the boundary layer (left and right, respectively). The outer expansion loses validity there. We rescale the problem near $z=0$ $(z=1)$ by setting $\zeta=\lambda z$ $[\chi=\lambda(z-1)]$, and express the various functions $\{\bar{c}_{K^+}^{(0)}(z),\bar{c}_{Cl^-}^{(0)}(z),\Phi^{(0)}(z)\}$ in terms of the new coordinates as $\{p^L(\zeta;1/\lambda),n^L(\zeta;1/\lambda),\phi^L(\zeta;1/\lambda)\}$, and $\{p^R(\chi;1/\lambda),n^R(\chi;1/\lambda),\phi^R(\chi;1/\lambda)\}$, in the left and right boundary layers, respectively. Next, considering the limit expansions obtained by holding ζ and χ fixed and letting $1/\lambda\to 0$, the problem can be solved in terms of the regular expansion $y_L^{(0)}(\epsilon,z)$ and $y_R^{(0)}(\epsilon,z)$.

3. Matching procedure

We choose four constants which allow that $y_L(\epsilon,z)$ and $y_{\text{outer}}(\epsilon,z)$, $y_R(\epsilon,z)$ and $y_{\text{outer}}(\epsilon,z)$, coincide for each order of the expansion in powers of ϵ (as $1/\lambda\to 0$) in some intermediate zone between the left boundary layer and the outer region, and the right boundary layer and the outer region, respectively. This yields

$$J_0=0,\quad C_0=2\pi c,$$

$$I_0=-C_0(1+\gamma)\Phi_R,\quad E_0=\frac{(1+\gamma)}{\gamma}\Phi_R,$$

$$J_1=\frac{1}{2}(2+\gamma)\pi\Phi_R,\quad C_1=\frac{\pi}{2\gamma}\Phi_R,$$

$$I_1=\frac{1}{12}\pi\gamma\Phi_R^2,\quad E_1=-\frac{(2+\gamma)\pi}{12C_0\gamma^2}\Phi_R^2. \tag{A4}$$

To obtain an approximate solution y_u that is valid *uniformly* on [0,1], we finally add the boundary and outer approximations and subtract their common limit in the intermediate zone.

[1] B. Alberts, D. Bray, J. Lewis, M. Raff, K. Roberts, and J. D. Watson, *Molecular Biology of the Cell* (Garland Publishing, New York, 2002).
[2] B. Hille, *Ionic Channels of Excitable Membranes* (Sinauer, Sunderland, MA, 1992).
[3] P. Yu. Apel, Y. E. Korchev, Z. Siwy, R. Spohr, and M. Yoshida, Nucl. Instrum. Methods Phys. Res. B **184**, 337 (2001); Z. Siwy, Y. Gu, H. A. Spohr, D. Baur, A. Wolf-Reber, R. Spohr, P. Apel, and Y. E. Korchev, Europhys. Lett. **60**, 349 (2002); Z. Siwy, A. Apel, D. D. Dobrev, R. Neumann, R. Spohr, C. Trautmann, and K. Voss, Nucl. Instrum. Methods Phys. Res. B **208**, 143 (2003).
[4] Z. Siwy, Y. C. Gu, H. A. Spohr, D. Baur, A. Wolf-Reber, R. Spohr, P. Apel, and Y. E. Korchev, Biophys. J. **82**, 266A (2002); Z. Siwy, P. Apel, D. Baur, D. D. Dobrev, Y. E. Korchev, R. Neumann, R. Spohr, C. Trautmann, and K.-O. Voss, Surf. Sci. **532-535**, 1061 (2003); Z. Siwy and A. Fuliński, Am. J. Phys. **72**, 567 (2004).
[5] E. A. Heins, Z. S. Siwy, L. A. Baker, and C. R. Martin, Nano Lett. **5**, 1824 (2005).
[6] C. C. Harrell, P. Kohli, Z. Siwy, and C. R. Martin, J. Am. Chem. Soc. **126**, 15646 (2004); A. Mara, Z. Siwy, C. Trautmann, J. Wan, and F. Kamme, Nano Lett. **4**, 497 (2004).
[7] Z. Siwy, L. Trofin, P. Kohli, L. A. Baker, C. Trautmann, and C. R. Martin, J. Am. Chem. Soc. **127**, 5000 (2005).
[8] S. Lee, Y. Zhang, H. S. White, C. C. Harrell, and C. R. Martin, Anal. Chem. **76**, 6108 (2004).
[9] Y. Choi, L. A. Baker, H. Hillebrenner, and C. R. Martin, Phys. Chem. Chem. Phys. **8**, 4976 (2006).
[10] A. E. Cardenas, R. D. Coalson, A. Nitzan, and M. G. Kurnikova, Biophys. J. **79**, 80 (2000).
[11] A. B. Mamonov, R. D. Coalson, A. Nitzan, and M. G. Kurnikova, Biophys. J. **84**, 3646 (2003).
[12] W. Im and B. Roux, J. Mol. Biol. **322**, 851 (2002).
[13] S. Yu. Noskov, W. Im, and B. Roux, Biophys. J. **87**, 2299 (2004).
[14] A. Alcaraz, E. M. Nestorovich, M. Aguilella-Arzo, V. M. Aguilella, and S. Bezrukov, Biophys. J. **87**, 943 (2004).
[15] M. B. Jackson, *Molecular and Cellular Biophysics* (Cambridge University Press, Cambridge, 2006).
[16] J. Keener and J. Sneyd, *Mathematical Physiology* (Springer, New York, 2001).
[17] R. Zwanzig, J. Phys. Chem. **96**, 3926 (1992).
[18] D. Reguera and J. M. Rubi, Phys. Rev. E **64**, 061106 (2001).
[19] D. Reguera, G. Schmid, P. S. Burada, J. M. Rubi, P. Reimann, and P. Hänggi, Phys. Rev. Lett. **96**, 130603 (2006).
[20] P. S. Burada, G. Schmid, D. Reguera, J. M. Rubi, and P. Hänggi, Phys. Rev. E **75**, 051111 (2007).
[21] A. M. Berezhkovskii, M. A. Pustovoit, and S. M. Bezrukov, J. Chem. Phys. **126**, 134706 (2007).
[22] C. L. Gardner, W. Nonner, and R. S. Eisenberg, J. Comput. Electron. **3**, 25 (2004).
[23] D. Gillespie and R. S. Eisenberg, Phys. Rev. E **63**, 061902 (2001).
[24] A. H. Nayfeh, *Perturbation Methods (Pure and Applied Mathematics)* (John Wiley and Sons, New York, 2000).
[25] D.-P. Chen, J. W. Jerome, R. S. Eisenberg, and V. Barcilon, SIAM J. Appl. Math. **57**, 631 (1997).
[26] R. A. Robinson and R. H. Stokes, *Electrolyte Solutions* (Butterworth, London, 1955).
[27] NAG Fortran Library Manual, *Mark 20* (The Numerical Algorithm Group Limited, Oxford, England, 2001).
[28] I. D. Kosińska, J. Chem. Phys. **124**, 244707 (2006).
[29] Z. Siwy and A. Fuliński, Phys. Rev. Lett. **89**, 198103 (2002); Z. Siwy, Adv. Funct. Mater. **16**, 735 (2006).
[30] K. T. Chu and M. Z. Bazant, Phys. Rev. E **74**, 011501 (2006).
[31] K. T. Chu and M. Z. Bazant, J. Colloid Sci. **315**, 319 (2007).
[32] M. S. Kilic, M. Z. Bazant, and A. Ajdari, Phys. Rev. E **75**, 021502 (2007).